

doi:10.15199/48.2018.11.34

Prototyping an MR damper system

Streszczenie. Tłumiki magnetoreologiczne (MR) należą do grupy semi-aktywnych urządzeń wykorzystujących tzw. ciecz inteligentne. Ciecz magnetoreologiczna jest zawieszoną cząstką ferromagnetycznych i należy do grupy materiałów o sterowalnych właściwościach reologicznych. Ciecz MR umieszczona w polu magnetycznym zmienia lepkość pozorną. Zmiana ta jest szybka i odwracalna, a końcowy stan materiału zależy od natężenia pola magnetycznego. Dzięki temu materiały te znalazły zastosowanie w semi-aktywnych układach redukcji drgań. Zaprojektowanie tłumika MR o odpowiednich osiągnięciach jest jednak zadaniem złożonym. W niniejszym artykule autor przedstawia koncepcję budowy modelu systemu MR obejmującego tłumik i regulator PWM. Na wybranym przykładzie przedstawiono wyniki obliczeń polowych magnetostatycznych i harmonicznym obwodzie tłumika. Wyniki obliczeń posłużyły m.in. do budowy modelu obwodu sterującego tłumika o parametrach skupionych z regulatorem. **Budowa modelu systemu MR obejmującego tłumik i regulator PWM.**

Abstract. Magnetorheological (MR) shock absorbers are semi-active devices based on smart fluids. The fluid when exposed to magnetic field undergoes a transition from a liquid to a pseudo-solid. The change is reversible and fast and it has made the material attractive for use in semi-active real-time systems for vibration reduction. At the same time designing a shock absorber is a complex process due to the multi-physics involved. In this paper the author shows an approach that can be used for virtual prototyping studies of MR flow-mode devices. Magnetostatic calculations are followed by time-harmonics analyses of the circuit of the valve. The analysis is then complemented by a parametric study of the controller-damper system subjected to regulated (commanded) current step inputs using a lumped parameter model of the MR valve.

Słowa kluczowe: tłumik MR, tłumik magnetoreologiczny, model polowy, model o parametrach skupionych, stany przejściowe.

Keywords: MR damper, magnetorheological damper, finite-element model, transient states.

Introduction

Flow-mode magnetorheological (MR) shock absorbers are exemplary semi-active devices utilizing so-called MR fluids. The fluid is a colloidal suspension of micron-size soft ferromagnetic particles [1]. The material when exposed to magnetic field develops a yield stress, thus undergoing a transition from a liquid to a pseudo-solid. The particles that are suspended in the carrier oil develop chain formations along the magnetic flux lines resulting in the resistance-to-flow build up. The change is reversible and fast. It is also of sufficient strength to merit the application of these fluids in real world devices, e.g. controllable vehicle dampers or powertrain mounts [2].

In general, MR dampers are free of mechanical valves with moving parts. Several advantages of MR dampers over conventional semi-active systems include continuously-variable damping characteristics, high damping force gain (ratio of the force in the off-state to the maximum force in the energized condition), low power draw, very good response times below 12 ms [3]. The technology has drawbacks, too. Fluid cost, sedimentation, durability are the challenges that the technology needs to cope with [4].

Still, designing an MR damper is an engineering challenge. It is mainly due to the nonlinearities involved between the output force and the input current. Several conflicting criteria often need to be met when developing a specific configuration of an MR damper system. For example, they are: low force in the non-energized state, high force in the energized condition, optimum response time, mass, packaging and the like [1,3].

Gołdasz and Sapiński [3] classified flow-mode MR valves in terms of the number of flow paths, flow path geometry, coil-core arrangement, asymmetry, fail-safe characteristics, etc. Analysis of commercial MR damper configurations shows that the majority of flow-mode devices feature one primary flow path, one or two coil assemblies wound onto a ferromagnetic core in the direction perpendicular to the fluid flow. Force asymmetry is usually realized by software means although designs with the asymmetric (rebound-to-compression) force characteristics exist. Same applies to fail-safe features and multiple parallel flow paths.

An integral part of the MR damper system is a power driver. Commercial (automotive) systems feature pulse-

with-modulation (PWM) amplifiers that offer low power consumption. The damper (plant) and the driver (controller) form a basic structure of a classic feedback (current) loop system [5] as shown in Fig. 1. Again, an inspection of the recent generation of the MagneRide system by BWI Group showed a switch from a previous generation current feedback control system to controllers with magnetic flux sensing capabilities [6]. Flux controllers offer benefits in terms of improved dynamics and effective cancelation of magnetic flux in the flow channel.

A suitable controller is not the only component of the MR damper system that influences the response time. There are several other factors: control coil inductance, MR fluid response, eddy currents in the magnetic structure [7]. The fluid's contribution is below 1 ms and can be neglected in transient model development. The impact of eddy currents is significant, however, it can be minimized by a careful selection of high resistivity materials or structural modifications of the valve's geometry [7,8]. At the same time the requirement for a low inductance (and faster) coil may degrade the steady-state output of the valve.

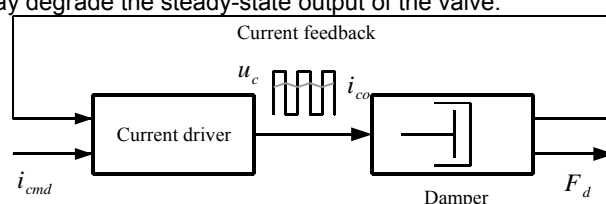


Fig. 1. MR damper system, i_{cmt} – current command, i_{co} – coil current, u_c – supply voltage, F_d – force [5]

The paper is organized as follows. First, the author proceeds with a series of magnetostatic finite-element calculations of the valve's magnetic circuit in order to estimate the steady-state output. That is followed by time-harmonic analyses of the presented configuration. Finally, the simulations are complemented by a parametric study involving the damper driven by a current controller.

MR valve

In this section the author reveals the configuration of an MR valve. The assembly that is shown in Fig. 2 shows one coil and one annular flow path. The geometry is presented

in Table 1. The core and the surrounding ring are made in ferromagnetic low carbon alloy steel grades, whereas the orientating plates are manufactured out of aluminum or stainless steel materials. The fluid in the annular gap is energized by the flux induced in the valve's structure. The induced flux passes through the core and into the annular gap, then into the outer ring to return to the core through the annular flow path again.

Moreover, the coil resistance is approximately 0.85Ω , and the number of coil turns is $N=100$. The wire size is 0.51 mm. The core's material is SAE 1010. Piston rod and the outer ring are made of the same material. The plates' material is the aluminum grade 6061-T6. The MR fluid's iron volume fraction is 26%, and their magnetization characteristic (B-H curve) is illustrated in Fig. 2.

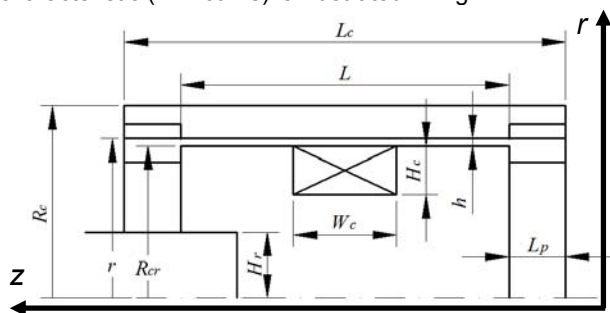


Fig.2. Geometry of a single coil MR valve assembly

Table 1. MR valve dimensions

Parameter	Value
Total length L_c	47 mm
Annular gap length L	35 mm
Coil width W_c	11 mm
Non-magnetic plate thickness L_p	6 mm
Coil height H_c	5.2 mm
Annular gap height h	0.8 mm
Core radius R_{cr}	16.2 mm
Surrounding ring (inner) radius r	17 mm
Outer radius R_c	20.5 mm
Rod radius H_r	7 mm

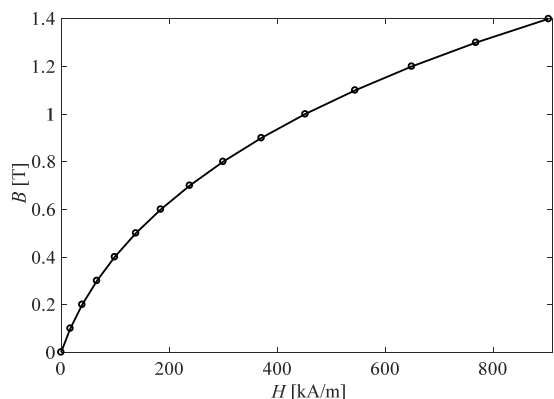


Fig.3. Magnetisation characteristics of the MR fluid [3], B – flux density, H – magnetic field strength

Magnetostatic analysis

In this section the author presents the results of finite-element (FE) magnetostatic analysis. In the analysis the geometry highlighted in Fig. 2 and Table 1 was used for developing a 2D axi-symmetric model of the valve with the software FEMM ver. 4.2. The results are revealed in Figs. from 3 to 7. In particular, Fig. 4 shows the flux density distribution in the valve at 100 ampere turns (see Fig. 4a) and 500 AT (ampere turns) (Fig. 4b). The results were obtained for the coil ampere turns up to $N=500$ AT. The

data at 500 AT also shows the flux bottleneck in the area below the coil window.

Analyzing the results shows, for example, that varying the ampere turns from 100 AT to 500 AT results in a threefold increase in the flux density level in the annular gap as shown in Fig. 5. Next, by averaging the flux density in the annular gap the flux density vs. coil ampere turns characteristics could be obtained – see Fig. 6.

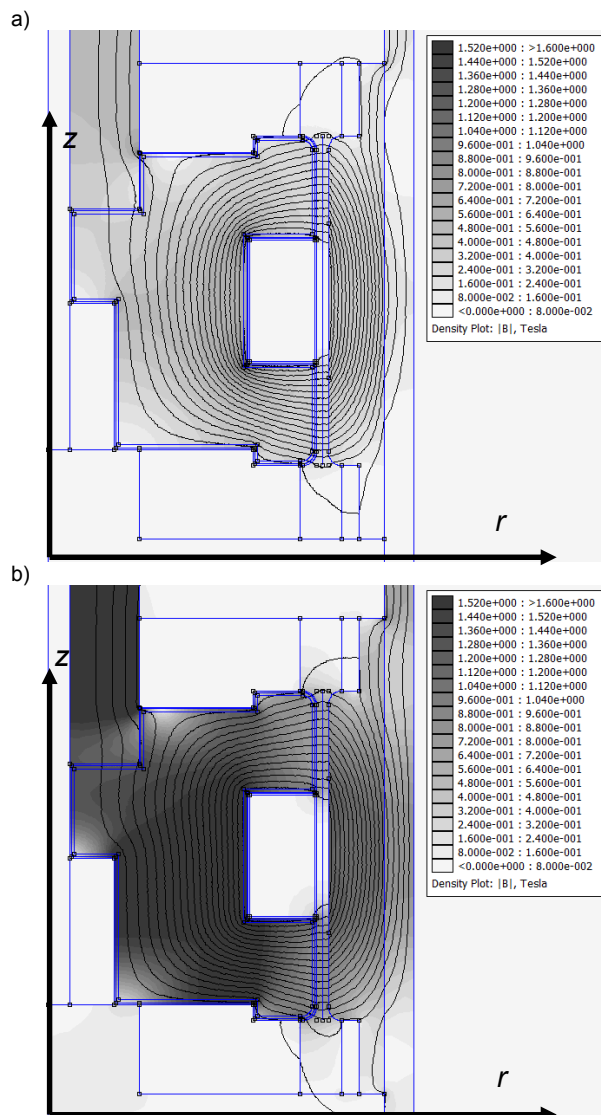


Fig.4. Flux density $|B|$ distribution and flux lines: a) 100 AT, b) 500 AT

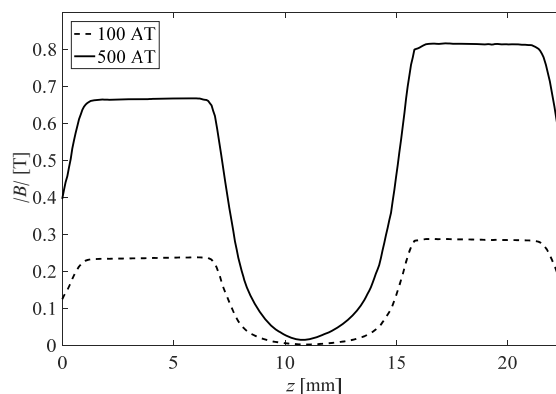


Fig.5. Computed flux density variation in the flow channel

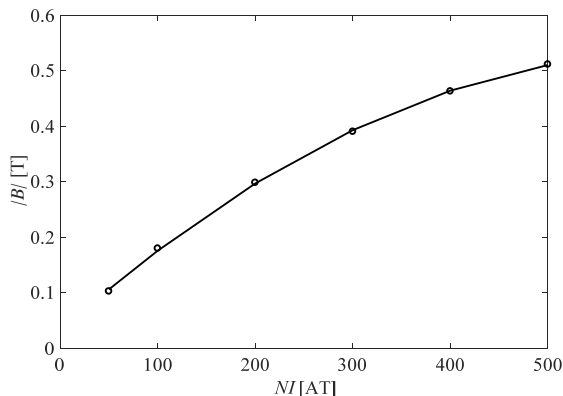


Fig. 6. Averaged flux density vs. coil ampere turns

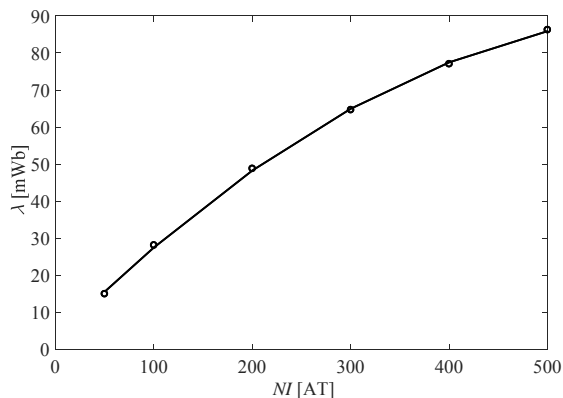


Fig. 7. Computed flux linkage vs. coil ampere turns

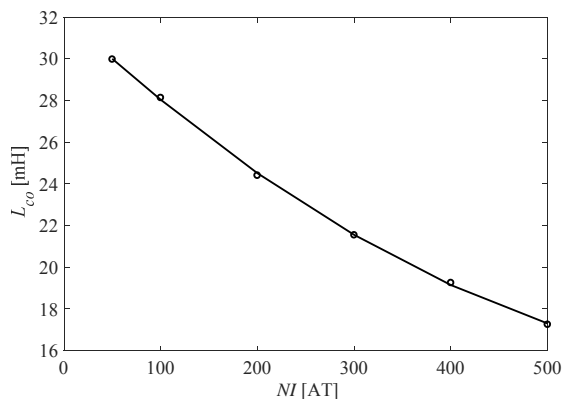


Fig. 8. Coil inductance vs. coil ampere turns

Also, Fig. 7 shows the computed flux linkage λ vs. coil ampere turns, and Fig. 8 reveals the evaluation of coil inductance. Specifically, the coil inductance variation range, e.g. from 28.13 mH (at 100 AT) to 17.25 mH (at 500 AT) justifies the use of the non-linear induction $L(i_{co})$ in transient state simulations of the control circuit in subsequent sections of this paper.

Time-harmonic analysis

In this section the results of the eddy current time-harmonics analysis are presented at input frequencies up to 50 Hz. The conductivity of SAE 1010 steel alloy (SAE 1010) was equal to 5.8 MS/m and that of aluminum plates equal to 24.59 MS/m. Throughout the analysis the examined current range was from 0 to 5 A (or 0 to 500 AT). It is assumed that the input current amplitude is maintained at the prescribed level regardless of the input's frequency so that only the impact of frequency f on magnetic field distribution can be computed and analyzed in more detail. The results are presented in Figs. 9 to 13. Briefly, increasing the input

frequency degrades the resulting flux density in the assembly – see Fig. 9. At 50 Hz the flux is not only confined to less than half space volume of the valve but its distribution in the flow channel and above the active sections is no longer uniform. As shown in Fig. 10 and Fig. 10c in particular the highest flux density can be located in the area near the coil window and decreasing toward the valve's ends. The observation is further enhanced when analyzing the relationship between averaged flux density vs. frequency in Fig. 11. The data in Fig. 11 clearly show that the effective flux density in the flow channel is nearly half of the static flux density level at the highest frequency.

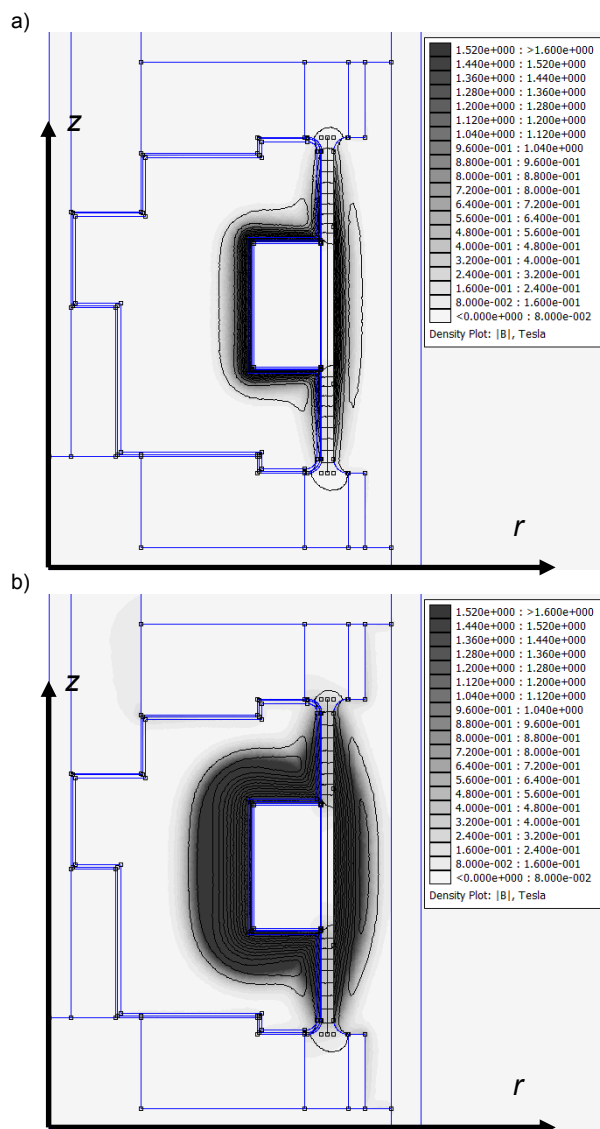


Fig. 9. Flux density distribution at $f=50$ Hz at: a) 100 AT turns, b) 500 AT

Moreover, examining the results revealed in Fig. 12 highlights the flux linkage degradation vs. frequency. The flux linkage vs. frequency plot shows similar relationship as that of flux density in Fig. 11. Finally, Fig. 13 highlights the (complex) inductance variation vs. input frequency and currents. Again, as in the DC case the inductance shows a strong dependence on the frequency. The calculated inductance includes a real part and an imaginary part. The imaginary part of the inductance L forms the real part of the circuit's impedance, whereas the imaginary part contributes to the real part of the impedance that is associated with frequency-dependent losses [9].

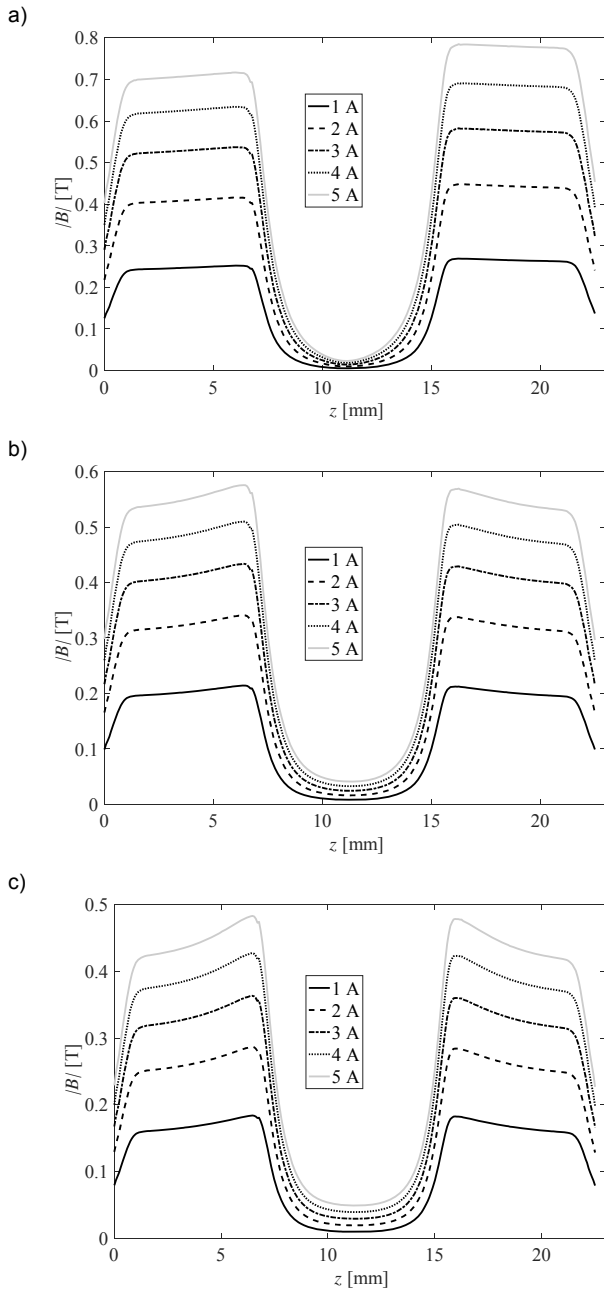


Fig. 10. Flux density vs. current in the flow channel at various frequencies: a) $f=5$ Hz, b) $f=25$ Hz, c) $f=50$ Hz.

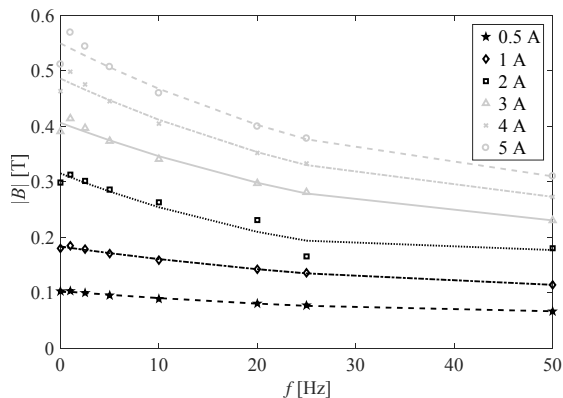


Fig. 11. Averaged flux density $|B|$ vs frequency f and current I_{co} .

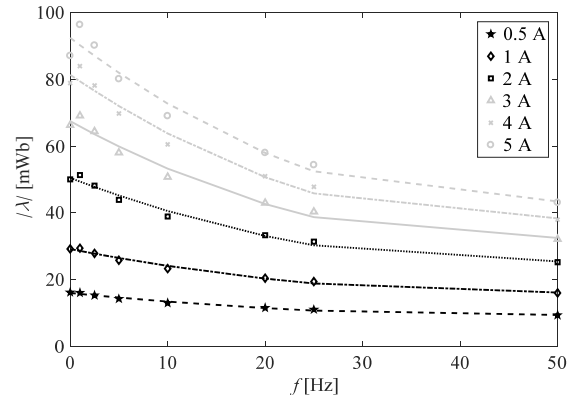


Fig. 12. Flux linkage vs. frequency and current

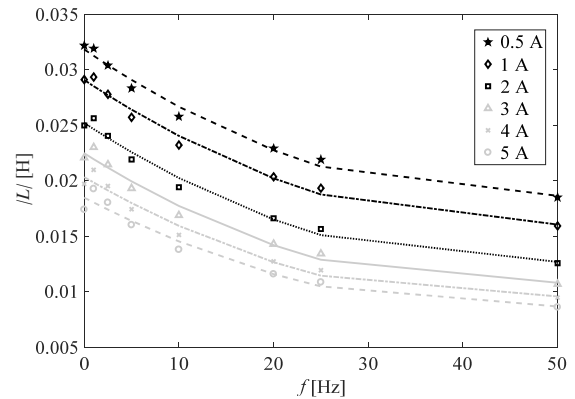


Fig. 13. Coil inductance vs. frequency and current

Controller-damper system simulations

In this section the authors illustrate the transient response of a closed loop system incorporating a current driver and a damper. The controller supplies the input voltage to the control coil of the damper. The current driver is a PWM (pulse width modulated) unit and it contains a PID regulator for controlling input signal's duty cycle. In this analysis the author utilizes the lumped parameter model of the control coil as highlighted in [10] (equations omitted here for the sake of brevity). As a remainder, the model utilized the control coil in the main loop and a secondary coil in the parasitic circuit (as a way of including the eddy currents in a simplified fashion). The nominal battery voltage is 12 V, and the remaining parameters of the circuit are as follows: $R_1=0.85 \Omega$ (main coil resistance), $R_2= 50 \mu\Omega$ (parasitic circuit resistance), $k=0.5$ (coil coupling factor), $L(I_{co})$ – see Fig. 8. The current driver is bi-polar, i.e. it is capable of the voltage $\pm 12V$. The impact of the driver model's parameters and those of the coil circuit model were studied through the simulations.

First, in Fig. 14 the influence of the supply voltage amplitude is illustrated. Predictably, increasing the input voltage accelerates the valve's response. Using the highlighted configuration of the controller augmenting the voltage level from the initial 12 V to 48 V resulted in decreasing the response time by a factor of appr. 2 albeit at the cost of the higher overshoot of the coil current. Next, in Fig. 15 the effect of turn-off voltage is presented. Here, the negative voltage is applied in the current decay phase of the commanded cycle. With this scenario increasing the turn-off voltage aid from 0 V to -11 V resulted in a significant acceleration of the current output of the valve down to appr. 10 ms from the overwhelming 90 ms in free-fall (0 V). Moreover, Fig. 16 reveals the current output with the anti-wind-up mechanism switched on in the controller.

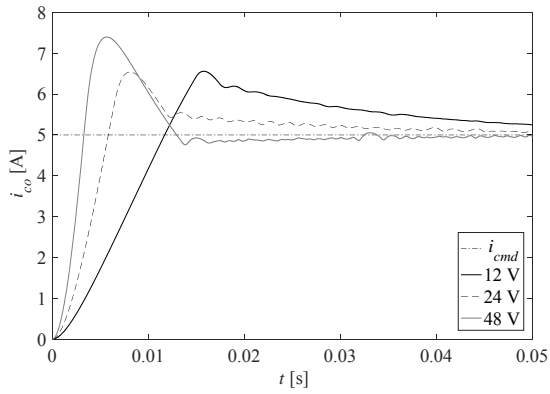


Fig. 14. Supply voltage impact ($I_{cmd}=5$ A, $K_p=10$, $K_i=50$, anti-windup: off)

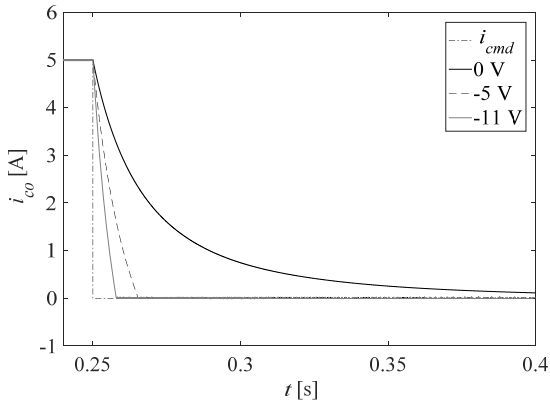


Fig. 15. Turn-off voltage impact ($I_{cmd}=5$ A, $K_p=10$, $K_i=50$, anti-windup: off)

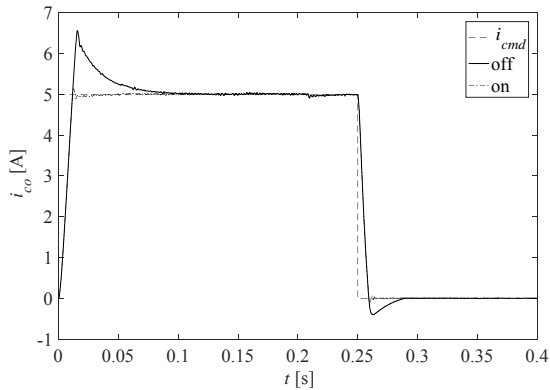


Fig. 16. PID component setting: anti-windup on/off ($I_{cmd}=5$ A)

The mechanism prevents the integration wind-up when in saturation. Activating the mechanism in the controller results in the elimination in the output current overshoot both in the current rise and current decay phases of the commanded current cycle. Finally, the data revealed in Figs. 17 to 19 illustrate the impact of the secondary (parasitic) circuit parameters on the performance of the valve. The parasitic circuit allows one to include the eddy current contribution to the actuator's output. Specifically, in Fig. 17 the author displays the results obtained by varying the coupling factor k . Here, increasing the coupling factor reduces the response time, however, at the cost of coil current oscillations. Next, the data shown in Fig. 18 reveal the current output variation with the parasitic circuit resistance R_{c2} . Including the parasitic resistance allows one to model the impact of the core material's conductivity. It can be observed that augmenting the parasitic resistance resulted in slowing down the secondary response of the actuator.

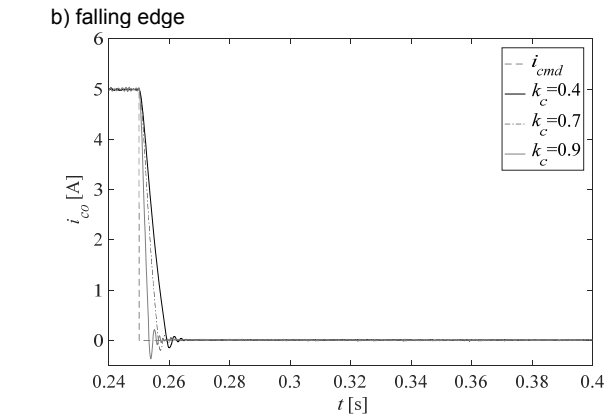
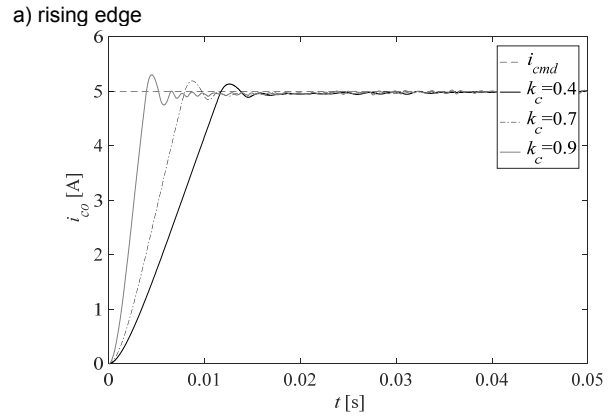


Fig. 17. Impact of the coupling factor k (anti-windup: on)

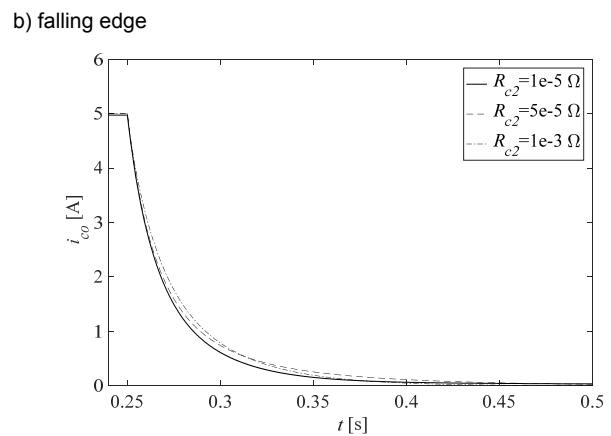
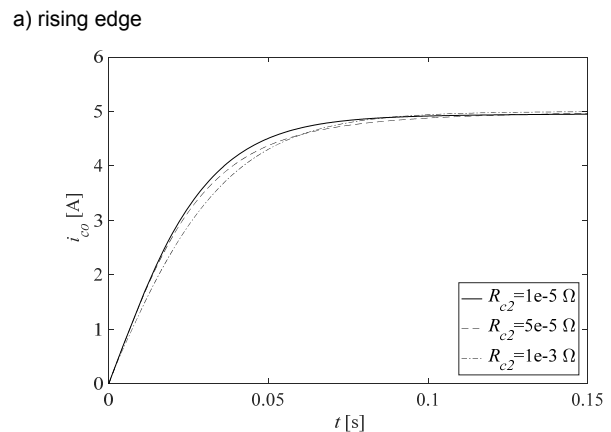


Fig. 18. Parasitic resistance impact: unregulated response ($k_c=0.4$)

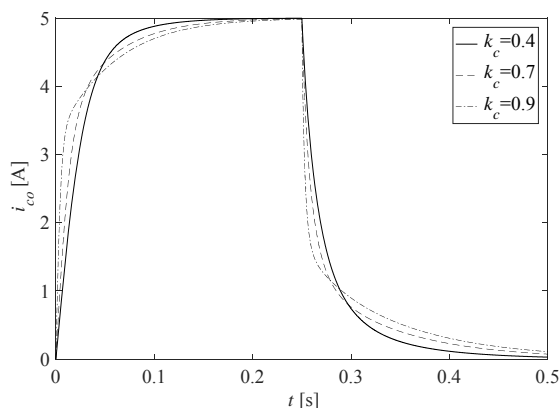


Fig. 19. Coil coupling factor: unregulated response ($R_2=50 \mu\Omega$)

Summary and conclusions

Designing an effective MR system incorporating a damper and a driver is a challenging task. It requires the consideration of various design parameters of different domains of engineering knowledge: magnetics, power electronics, non-Newtonian fluid dynamics, etc.

In the paper the author reveals an approach that can be used to study the steady-state and transient response of an MR damper. The author starts with the development of a magnetostatic model of the control valve in order to acquire the information on the steady-state output. The calculated non-linear coil inductance-current characteristic is then input into the lumped parameter model of the valve. The valve's analysis is then complemented by time-harmonic calculations. Based on the obtained data it is then apparent that the input signal frequency has a significant and negative impact on the output of the valve.

Future works will concentrate on the development of a higher order eddy current mechanism and incorporating it into the control coil model. Exploring the magnetic hysteretic behaviour of MR valves is planned in near future, too. The steps are necessary for developing a high-bandwidth model of the actuator. The complete model can be then used not only for rapid prototyping studies of MR valves and control algorithms but also in studies on electrical interfaces as in [11].

The author wishes to acknowledge the support of the statutory grant no. E3/611/2018/DS funded by Cracow University of Technology.

Author: mgr inż. Paweł Trębacz, Instytut Automatyki i Trakcji Elektrycznej, Wydział Inżynierii Elektrycznej i Komputerowej, Politechnika Krakowska, ul. Warszawska 24, 31-155 Kraków, E-mail: pawel.trebacz8@gmail.com.

REFERENCES

- [1] Carlson J.D., Catanzarite D.M., St. Clair K.A., Commercial magneto-rheological fluid devices., *International Journal of Modern Physics B*, 10 (1996), no. 23-24, 2857-2865
- [2] Jolly M.R., Bender J.W., Carlson J.D., Properties and applications of commercial magnetorheological fluids., *Journal of Intelligent Material Systems and Structures*, 10 (1999), no. 1, 5-13
- [3] Goldasz J., Sapiński B., Insight into Magnetorheological Shock Absorbers, *Springer International Publishing* (2015)
- [4] Carlson J.D., What makes a good MR fluid?, *Journal of Intelligent Material Systems and Structures*, 13 (2002), no. 7-8, 431-435
- [5] Choi S.B., Li W., Yu M., Du H., Fu J., Do P.X., State of the art of control schemes for smart systems featuring magneto-rheological materials., *Smart Materials and Structures*, 25 (2016), no. 4, 043001
- [6] Nehl T.W., Gopalakrishnan S., Deng F., Direct flux control system for magnetic structures, *U.S. Patent Application No. 11/451,935*
- [7] Kubik M., Machacek O., Strecker Z., Roupec J., Mazurek I., Design and testing of magnetorheological valve with fast response time and great dynamic force range., *Smart Materials and Structures*, 26 (2017), 047002
- [8] Strecker Z., Roupec J., Mazurek I., Machacek O., Kubik M., Klapka M., Design of magnetorheological amper with short time response, *Journal of Intelligent Material Systems and Structures*, 26 (2015), no. 17, 1951-1958
- [9] Mayer D., Ulrych B., Complex inductance and its computer modelling., *Journal of Electrical Engineering*, (2002), no. 1-2, 24-29
- [10] Goldasz J., Dzierzak S., Parametric study on the performance of automotive MR shock absorbers., *In IOP Conference Series: Materials Science and Engineering*, (2016), no. 1, 012004
- [11] Jastrzębski Ł., Sapiński B., Electrical interface for an MR damper-based vibration reduction system with energy harvesting capability, *In Proceedings of the International Carpathian Control Conference*, (2017), 189-192, doi:10.1109/CarpathianCC.2017.7970395